Spatial Heterogeneity of Air–Sea Energy Fluxes over a Coral Reef—Heron Reef, Australia

MELLISSA C. MACKELLAR, HAMISH A. MCGOWAN, AND STUART R. PHINN

University of Queensland, Brisbane, Queensland, Australia

(Manuscript received 15 June 2011, in final form 9 January 2012)

ABSTRACT

The thermal environment of a coral reef is moderated by complex interactions of air–sea heat and moisture fluxes, local to synoptic-scale weather and reef hydrodynamics. Measurements of air–sea energy fluxes over coral reefs are essential to understanding the reef–atmosphere processes that underpin coral reef environmental conditions such as water temperature, cloud, precipitation, and local winds (such as during coral bleaching events). Such measurements over coral reefs have been rare, however, and the spatial heterogeneity of surface–atmosphere energy exchanges due to the different geomorphic and biological zones on coral reefs has not been captured. Accordingly, the heterogeneity of coral reefs with regard to substrate, benthic communities, and hydrodynamic processes has not been considered in the characterization of the surface radiation budget and energy balance of coral reefs. Here, the first concurrent in situ eddy covariance measurements of the surface energy balance and radiation transfers over different geomorphic zones of a coral reef are presented. Results showed differences in radiation transfers and sensible and latent heat fluxes over the reef, with higher Bowen ratios over the shallow reef flat zone. The energy flux divergence between sites increased with wind speed and during unstable, southeasterly trade winds with the net flux of heat being positive and negative over different geomorphic zones. The surface drag coefficient at measurement height ranged from 1×10^{-3} to 2.5×10^{-3}, with no significant difference between sites. Results confirm that spatial variation in radiation and air–reef–water surface heat and moisture fluxes occurs across a lagoonal platform reef in response to local meteorological conditions, hydrodynamics, and benthic–substrate cover.

1. Introduction

Exchanges of heat, moisture, and momentum across the air–sea interface set up heat and moisture gradients that drive regional atmospheric and oceanic circulations (Hasse and Smith 1997). Accurate measurement of these fluxes is essential to understanding the processes that underpin local air and water surface temperatures, humidity, air pressure, and cloud fields in coastal and marine settings (Stammer et al. 2004). They are also necessary to parameterize and validate regional to global-scale forecast models to improve prediction of weather and climate (Beyrich et al. 2002; Hasse and Smith 1997).

Coral reefs cover approximately 2.8×10^5–6.0×10^5 km^2 of Earth's surface (Hoegh-Guldberg et al. 2007) and are a major source of heat and moisture to the atmospheric boundary layer thereby affecting cloud field properties, local winds, rainfall, and cyclone genesis (Garratt and Hyson 1975; Krishna and Rao 2009). The complexities of making micrometeorological measurements over coral reefs have long been a deterrent to researchers, however, and there remains a dearth of information on coral reef surface energy balance and radiation transfers.

To date, research has principally focused on the measurement of energy exchanges over the open ocean made from instrumented buoys or ships (Fairall et al. 1996; Large and Pond 1981; Smith et al. 1992). Because of its large heat storage capacity, the open ocean is a sink or source of energy, depending on the diurnal solar cycle and hydrodynamics (Arya 2001). Over the western tropical Pacific Ocean, the net heat flux into the water was found to represent 40% of available net radiation Q^* (Tsukamoto and Ishida 1995). The high level of available moisture over oceans means latent heat flux (water vapor flux between the surface and atmosphere) dominates over sensible heat (heat flux into the overlying air) and, typically, annual values of the Bowen

Corresponding author address: M. MacKellar, Climate Research Group, School of Geography, Planning and Environmental Management, Chamberlain Building (35), Level 4, Rm. 408, St. Lucia Campus, University of Queensland, Campbell Road, Brisbane QLD 4072, Australia.
E-mail: m.mackellar@uq.edu.au

DOI: 10.1175/JAMC-D-11-0120.1

ratio β, the ratio of sensible heat Q_H to latent heat flux Q_E, are low, at approximately 0.10 (Oke 1978). At Heron Reef on the southern Great Barrier Reef (GBR), values of β ranging from 0.04 to 0.17 have been measured (MacKellar and McGowan 2010; McGowan et al. 2010), while downwind from a submerged coral plateau in the East China Sea β as high as 0.2 were reported by Garratt and Hyson (1975). Evidently, energy fluxes over shallow warm coral reefs vary significantly and differ from those over the open ocean.

Net radiation (the sum of incoming and outgoing short- and longwave radiation) over coral reefs is typically lower than over the surrounding tropical ocean, because of the higher albedo (light scattering) of the reef surface, typically with a higher proportion of Q^* being absorbed into the water column (McGowan et al. 2010; Tanaka et al. 2008). Consequently, coral reefs are subject to enhanced heating, due to the lower thermal capacity of the shallower water column relative to the surrounding ocean (Nihei et al. 2002).

Research into the surface energy balance of coral reefs from in situ measurements has been rare. Rather, energy exchanges over coral reefs have been computed indirectly (McCabe et al. 2010) and have focused on the development of bulk transfer algorithms from shoreline measurements made from towers (Fairall et al. 1996; Francey and Garratt 1979; Garratt and Hyson 1975) and/or have relied on shipboard measurements (Tsukamoto et al. 1995). McCabe et al. (2010) used bulk formulas to compute the turbulent fluxes (Q_E and Q_H) over the reef flat at Lady Elliot Island in the southern GBR, during autumn (April). They found that Q_E averaged 150 W m^{-2} and increased to 250 W m^{-2} during windy periods. Garratt and Hyson (1975) measured vertical fluxes of momentum, Q_H and Q_E, downwind of a coral reef during a cold-air outbreak in winter in the South China Sea. Under these conditions, Q_E and Q_H reached as high as 550 and 110 W m^{-2}, respectively. This highlighted wind speed and the air–reef–water temperature difference as key controls of the turbulent fluxes over coral reefs.

Tanaka et al. (2008) measured radiation and turbulent fluxes directly with a mast-mounted eddy covariance (EC) system, downwind of a coral reef in late summer. They found the mean Q_H to be small at 6 W m^{-2}, while the mean Q_E was 60 W m^{-2}. Net radiation averaged 223 W m^{-2} and overall during their observation period the reef acted as an energy sink. Recently, EC measurements of the surface energy balance over Heron Reef, in the southern GBR, have provided rare insight into the diurnal partitioning of the surface energy balance (McGowan et al. 2010). This research showed that over the shallow reef flat >80% of daytime available Q^* was partitioned into the water column, benthos, and substrate (called Q_{SWR}), and that incident shortwave radiation $K\downarrow$ was moderated by the presence of cloud cover that, in addition to regional meteorological conditions, may be affected by dimethylsulfide (DMS) emitted from the coral reefs (Charlson et al. 1987; Jones et al. 2007). During February 2009, MacKellar and McGowan (2010) recorded $K\downarrow$ over Heron Reef in excess of 1000 W m^{-2} under cloud-free conditions. High levels of solar radiation, in conjunction with suppressed evaporative cooling due to low wind speeds, resulted in intense heating of the water overlying the reef, particularly during midday low tides, which caused localized coral bleaching.

While these previous studies provided the first direct insight into the surface energy balance of coral reefs, they use single-point measurements to make inferences of the micrometeorology of coral reefs at reef scale. Coral reefs are characterized by distinct geomorphic zones, however, with varying bathymetry, hydrodynamics, and benthic assemblages producing different and dynamic albedos (Gourlay 1996). Thus, single-point measurements can only be considered representative of the geomorphic zone(s) and benthic communities on a reef within the footprint of their measurements.

In this paper we present results from the first simultaneous measurements of the surface energy balance at different locations across a coral reef using EC. Measurements were made over three geomorphic zones at Heron Reef in the southern GBR, Australia, and the adjacent open ocean for 4–13 February 2010 (austral summer). This study provides the first insight into spatial variation of air–reef–water surface energy fluxes over a coral reef.

2. Site description

Covering 27 km^2, Heron Reef lies approximately 80 km northeast of Gladstone, on Australia's east coast, near the Tropic of Capricorn (Fig. 1). It is a typical lagoonal platform reef, formed on an antecedent karst platform with episodic growth corresponding with higher sea levels during Holocene sea level fluctuations (Hopley et al. 2007). Heron Reef shares similar hydrology, bathymetry, geology, and morphology with the other platform reefs in the southern GBR region (Jell and Flood 1978). Heron Island, on the western end of the reef, is 800 m long and 280 m wide and is a maximum of 5.6 m above sea level. The coral cay supports a large stand of *Pisonia grandis* forest, a resort, and a research station. Within 1 km to the southwest of Heron Reef, a 25-m-deep channel separates Heron Reef from Wistari Reef, while to the east and southeast two other reefs are present: Sykes and One Tree Reef.

With a spring and neap tidal range of 2.28 and 1.09 m, respectively (Chen and Krol 1997), tides are semidiurnal

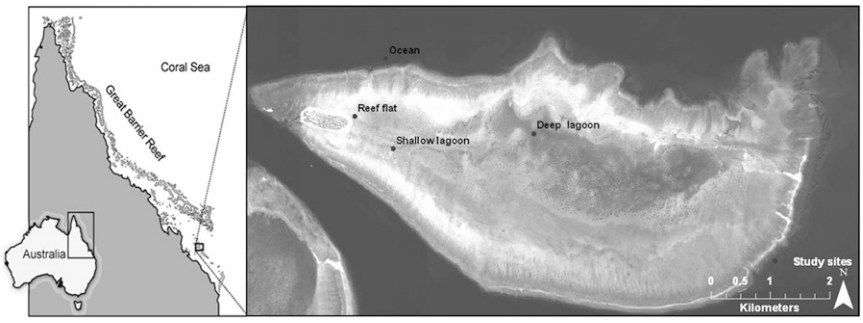

FIG. 1. Heron Island and Reef location map. (Quickbird-2 image at 0028:20 UTC 3 Aug 2006 provided by DigitalGlobe and Centre for Spatial Environmental Research.)

and, under an average wind speed of 5 m s^{-1} and wave height of 0.5 m, the mean maximum current velocity across the reef flat is 0.3 m s^{-1} (Gourlay and Hacker 1999). Wave action at Heron Reef is typically less than 0.6 times the maximum water level (Gourlay 1996). Local wave properties are influenced by the regional wave climate when the tide is higher than the reef rim and oceanic waves move across the reef top. Southeast trade winds are prevalent along the east coast and result in low to moderate seas, occasionally with sea-breeze waves superimposed on them. During February at the Emu Park Waverider buoy, northwest of Heron Reef, the average significant wave height is approximately 0.95 m with the dominant wave direction from the northeast (DERM 2004). Although formal estimates of flushing rates are not yet available for Heron Reef, preliminary modeling by the Commonwealth Scientific and Industrial Research Organisation (CSIRO) indicates that bathymetry, tidal flows, wind direction, wind speed, and wave action influence the drag and mixing imparted by the benthos and substrate and determine residence time. Flushing rates are typically higher on the windward side(s) and in shallower areas (outer and inner reef flat), noting that these change with predominant wind directions. Residence times are highly variable due to short-term changes in these forcing factors.

Irradiance over the Capricorn Bunker region varies seasonally with the highest average daily irradiance in summer (>30 MJ m^{-2} day^{-1}), followed by autumn, spring, and winter, respectively (Masiri et al. 2008). As a result of the positioning of the subtropical high pressure zones, Heron Reef lies in the latitudinal region in the southern GBR where the maximum summer and autumn solar irradiances occur. Masiri et al. (2008) showed that regions of maximum solar radiation coincide with areas of maximum coral bleaching, as exemplified during the 2002 mass coral bleaching event. Coral reefs in the vicinity of the southern GBR are, therefore, vulnerable to coral bleaching. Though not measured here, the optical properties of the water on the reef vary depending on the tide and weather, affecting the water column temperature and reflectivity. Studies have shown that the incoming tide floods the lagoon with water from the surrounding ocean, often with high phytoplankton content, producing greener waters. As the water drains from the reef top at low tide, the water often appears ''whiter'' (higher albedo) due to higher concentrations of nonliving suspended particulate matter, particularly when windy conditions increase the mixing of water on the reef (Wettle et al. 2005). Optical thickness and constituents of the water column affect its ability to conduct and store energy. This is important when considering absorption, scattering, and transmission of light of different wavelengths in the water column and should be considered in future work.

Mean air temperature on Heron Island at 1500 eastern standard time (EST) varies from 28.3°C in January to 20.1°C in July (Bureau of Meteorology 2011). Rainfall is bimodal with an annual mean of 1050 mm, falling predominantly during summer and autumn. Southward dips in the intertropical convergence zone during summer can result in heavy rainfall at Heron Reef associated with convectively unstable air masses (Sturman and McGowan 1999). The southeast trades are the dominant winds at Heron Reef, with a winter westerly component associated with the repositioning of the prevailing synoptic weather systems. Wind direction is more variable in summer with greater prevalence of warm northerly winds.

Heron Reef has been classified into geomorphic zones with distinctive hydrodynamic and geomorphic characteristics, as well as benthic assemblages (Jell and Flood 1978; Ahmad and Neil 1994; Andrefouet and Payri 2001). We used the most recent data, which are the only ones with field validation and provide a representation of distinct zones of substrate–benthos and process assemblages at the time of our field work (Phinn et al. 2011). Table 1 details the benthic assemblages of the reef flat and shallow and deep lagoon sites, which, respectively, cover 32%,

TABLE 1. The EC system locations and benthic assemblage for the three OPs.

Obs period	Period	Unit	Position	Benthic assemblage	Total reef area (%)
1	0000 UTC 4 Feb 2010–0500 UTC 7 Feb 2010	EC1	Shallow reef flat	Sand (21%), algae (28%), rubble and sand (48%), benthic microalgae (1.8%), live coral (0.2%)	32
		EC2	Shallow lagoon	Sand (52%), bommies (2.5%), rubble (0.5%), benthic microalgae (45%)	16
2	0530 UTC 7 Feb 2010–0700 UTC 12 Feb 2010	EC1	Shallow reef flat	Sand (21%), algae (28%), rubble and sand (48%), benthic microalgae (1.8%), live coral (0.2%)	32
		EC2	Deep lagoon	Bommies (21%), sand (79%)	13
3	0730 UTC 12 Feb 2010–1230 UTC 13 Feb 2010	EC1	Shallow reef flat	Sand (21%), algae (28%), rubble and sand (48%), benthic microalgae (1.8%), live coral (0.2%)	32
		EC2	Open ocean	—	—

16%, and 12% of the total reef surface. The remaining area of Heron Reef is composed of the outer reef flat, reef slope, reef crest, and the coral cay, which cover 20%, 13%, 6%, and 1%, respectively.

3. Instrumentation

Surface energy balance and radiation measurements were made over Heron Reef and the adjacent ocean using EC systems mounted on two pontoons (Weibe et al. 2011; McGowan et al. 2010). Eddy covariance unit 1 (EC1) was installed approximately 50 m offshore from the eastern end of Heron Island in the shallow reef flat zone (23.443°S, 151.921°E) where it operated for the entire study period. A second EC unit (EC2) alternated between the other sites. From 0000 EST 4 February to 0500 EST 7 February 2010, EC2 was located in the shallow lagoon (23.446°S, 151.927°E), from 0530 EST 7 February 2010 to 0700 EST 12 February 2010 EC2 was at the deep lagoon site (23.444°S, 151.951°E), and for a 28-h period from 0730 EST 12 February until 1230 EST 13 February EC2 was installed at an ocean site (23.433°S, 151.925°E), off the northern edge of the reef rim.

Each EC unit consisted of a Campbell Scientific CSAT-3 sonic anemometer (accuracy of $U_x < \pm 4.0$ cm s^{-1} and of U_y and $U_z < \pm 2.0$ cm s^{-1}), a Li-Cor CS7500 open-path H_2O and CO_2 analyzer (accuracy is within 2% of reading), a Kipp and Zonen CNR1 net radiometer (spectral range of 0.3–50 μm and response time < 18 s), and a Vaisala HMP45A sensor (accuracy of ±0.2°C for air temperature and ±2.5% for relative humidity) recorded ambient air temperature and humidity. All instruments were fixed at a constant height of 2.2 m above the water surface and were connected to a Campbell Scientific CR3000 datalogger with measurements made at 10 Hz with 15-min block averages logged. Water level was recorded using HOBO U20-001-01 water-level monitors (accuracy of 0.21 cm and ±0.37°C at 20°C), and the near-surface water temperature at a depth of 0.05 m below the surface was monitored using a HOBO water temperature PROV2 logger (accuracy of ±0.2°C) on EC1 and a Campbell Scientific model 107 temperature probe (<±0.2°C over 0°–50°C) on EC2. A Vaisala CL-51 ceilometer logged cloud-base height continually throughout the field campaign with a reporting range of 7.5 km at a resolution of 10 m. Instrumentation was factory calibrated and daily services were performed to ensure sensors were level and free from salt scale. Turbulent fluxes are not influenced by measurements from the HMP45A sensor. Eddy covariance measurement error was believed to be approximately 10%–15% from terrestrial studies (e.g., Allen et al. 2011).

Prior to deployment, the EC units were run side by side on the beach allowing cross calibration of sensors, and showed good agreement in the radiation data. During this period incoming shortwave varied by an average of 1.15%, while incoming longwave radiation varied by 0.3% and outgoing longwave radiation varied by 0.11% between the two systems. Weibe et al. (2011) demonstrated that, over the averaging period used here, the effect of small-scale perturbations of wave-induced motion are not considered to affect flux measurements. Accordingly, calculations of Q_H and Q_E are considered to accurately reflect turbulent energy fluxes at specific locations over the reef–water surface at Heron Reef (McGowan et al. 2010).

4. Methods

The surface energy balance for Heron Reef was written as

$$Q^* = Q_E + Q_H + \Delta Q_S + \Delta Q_A + Q_R + Q_G, \qquad (1)$$

where Q^* = net all-wave radiation, Q_E = latent heat flux, Q_H = sensible heat flux, ΔQ_S = change in heat storage of the layer of water overlying the coral reef, ΔQ_A = net horizontal advection of heat in the water by

TABLE 2. Flux footprint model input parameters.

Obs period	Site	Roughness length (m)	Wind direction	Obukhov length (m)	Stability classification	Std dev of wind direction (°)	Friction velocity (m s^{-1})
1	Reef flat	0.000 20	NE	−1253	Unstable	8.5	0.36
	Shallow lagoon	0.000 38	NE	−234	Unstable	8.5	0.35
2	Reef flat	0.000 18	SE	−1757	Unstable	7.6	0.49
	Deep lagoon	0.000 21	SE	−473	Unstable	7.5	0.44
3	Reef flat	0.000 31	NE	−2477	Unstable	8.2	0.34
	Ocean	0.000 19	NE	−1039	Unstable	8.1	0.34

currents, Q_R = addition or loss of heat associated with rainfall, and Q_G = heat transfer via conduction and radiation transfers into or out of the reef substrate (McGowan et al. 2010). Rain-effected measurements were removed for the measurement periods reported here, so Q_R was removed from Eq. (1). As measurements of horizontal advection of heat over the reef by currents and the partitioning of heat into the reef benthos and substrate were not made, for the purpose of this study, these parameters were grouped (ΔQ_{SWR}) and collectively determined as the residual of the equation. This approach is used when direct measurement of energy transfer through the water column and/or underlying substrate, including coral, is not practical (Kurasawa et al. 1983; MacKellar and McGowan 2010; McGowan et al. 2010; Tsukamoto et al. 1995). As a result, the surface energy balance equation for Heron Reef was rewritten as

$$Q^* = Q_H + Q_E + \Delta Q_{\mathrm{SWR}}. \qquad (2)$$

Post–data processing of the energy flux data included corrections for frequency attenuation (Massman and Lee 2002), density effects (Webb et al. 1980), two-dimensional coordinate rotation (Lee et al. 2004), and spike removal. The source area footprint of the measured turbulent fluxes was calculated using a model developed by Isaac (2004), which employs the Horst and Weil (1992) model for the crosswind component and functions for predicting the upwind dimension by Schmid (1994). This widely used approach was chosen because it includes the stability correction function (ψ_m, defined below) and provides a reliable 3D representation of the flux source area. The roughness length Z_0 was calculated following Abdella and D'Alessio (2003). The input parameters for the footprinting model are listed in Table 2 and the resulting 80% isopleth footprints are plotted in Fig. 2. The upwind distance of the 80% isopleth during observation periods 1, 2, and 3 (OP1, OP2, and OP3) were 433, 437, and 409 m for the reef flat, respectively; 392 and 429 m for the shallow and deep lagoons; and

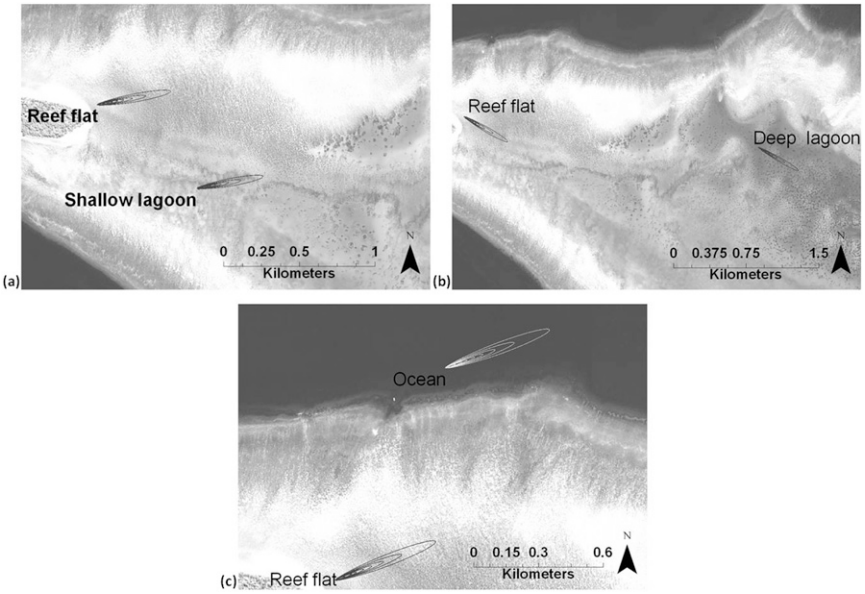

FIG. 2. Measurement footprints for the (a) reef flat and shallow lagoon sites during OP1, (b) reef flat and deep lagoon during OP2, and (c) reef flat and open-ocean site during OP3.

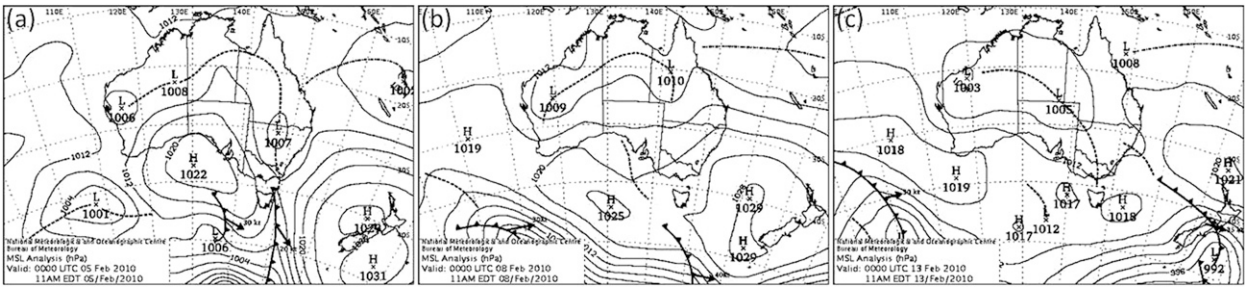

FIG. 3. Representative mean sea level pressure analysis charts for Australia for (a) OP1 on 5 Feb, (b) OP2 on 8 Feb, and (c) OP3 on 13 Feb 2010.

436 m for the open ocean. The area of maximum influence on the EC measurements at the surface ranged from 32 to 35 m upwind of the measurement sites. The footprints were larger on the reef flat during OP1 and OP2 because of the smaller Obukhov and Z_0 lengths at the sites. It is likely that the shallow and deep lagoons had slightly higher Z_0 values than the reef flat because of continuous deep water coverage and greater wave action. During OP3, Z_0 was smaller over the ocean and, hence, the footprint extended farther upwind.

The drag coefficient C_D at the measurement height of 2.2 m was calculated according to Hsu (1988) as

$$C_D = C_{DN}\left[1 - \frac{\psi_m(Z/L)}{\ln(Z/Z_0)}\right]^{-2}, \tag{3}$$

where z is the measurement height, L is the Monin–Obukhov length, and C_{DN} is the drag coefficient for neutral conditions:

$$C_{DN} = \left[\frac{k}{\ln\left(\frac{Z}{Z_0}\right)}\right]^{-2}. \tag{4}$$

Under unstable conditions,

$$\psi_m = \ln\left[\left(\frac{1+X^2}{2}\right)\left(\frac{1+X}{2}\right)^2\right] - 2\arctan X + \frac{\pi}{2},$$

$$\text{where} \quad X = (1 - 16Z/L)^{1/4}, \tag{5}$$

and, under stable conditions,

$$\psi_m = -5\frac{Z}{L}. \tag{6}$$

The 10-m neutral drag coefficient was also calculated to facilitate comparison with previously reported drag coefficients, following Stull (2000).

5. Results

a. Local meteorology

Observation periods 1–3 were characterized by contrasting local to synoptic-scale conditions. At the start of OP1 east-northeasterly winds (averaging 80°) persisted at around 7 m s^{-1} under the influence of a surface trough (Fig. 3a), bringing a moist, unstable air mass over Heron Reef. This resulted in convective shower activity on 4 February 2010. After midday the wind speed decreased and remained at an average of 4.3 m s^{-1} on 5 and 6 February (Fig. 4). This was due to a weaker synoptic pressure gradient affecting Heron Reef as the trough moved farther away. Overall, the average air temperatures at the reef flat and shallow lagoon measurement sites were similar at 26.7° and 26.5°C, respectively, while the average absolute humidities were 19.4 and 18.8 g m^3, respectively (Table 3).

During OP2 an anticyclone off southeastern Australia (Fig. 3b) resulted in stronger southeasterly winds from around 120° with a mean wind speed of 7.0 m s^{-1}. Convective rain cells continually developed, resulting in 24.2 mm of rainfall during the 121.5-h measurement period. The majority of the precipitation fell on 7 and 8 February 2010; however, strong southeasterlies and unstable conditions prevailed throughout OP2. Air temperatures were similar to those during OP1 and the absolute humidity was slightly higher, at 19.9 g m^3 (Table 3). During OP3, weak northeasterly winds at an average of 5 m s^{-1} were measured with clear conditions prevailing and no rainfall recorded. Mean air temperature was the highest at 27°C. The Monin–Obukhov length L is a parameter that determines stability in the surface layer (Launiainen 1995) and is important for determining the EC measurement footprint. Calculations of L were conducted for the entire field measurement campaign and confirmed that unstable boundary layer conditions prevailed at Heron Reef during the daytime.

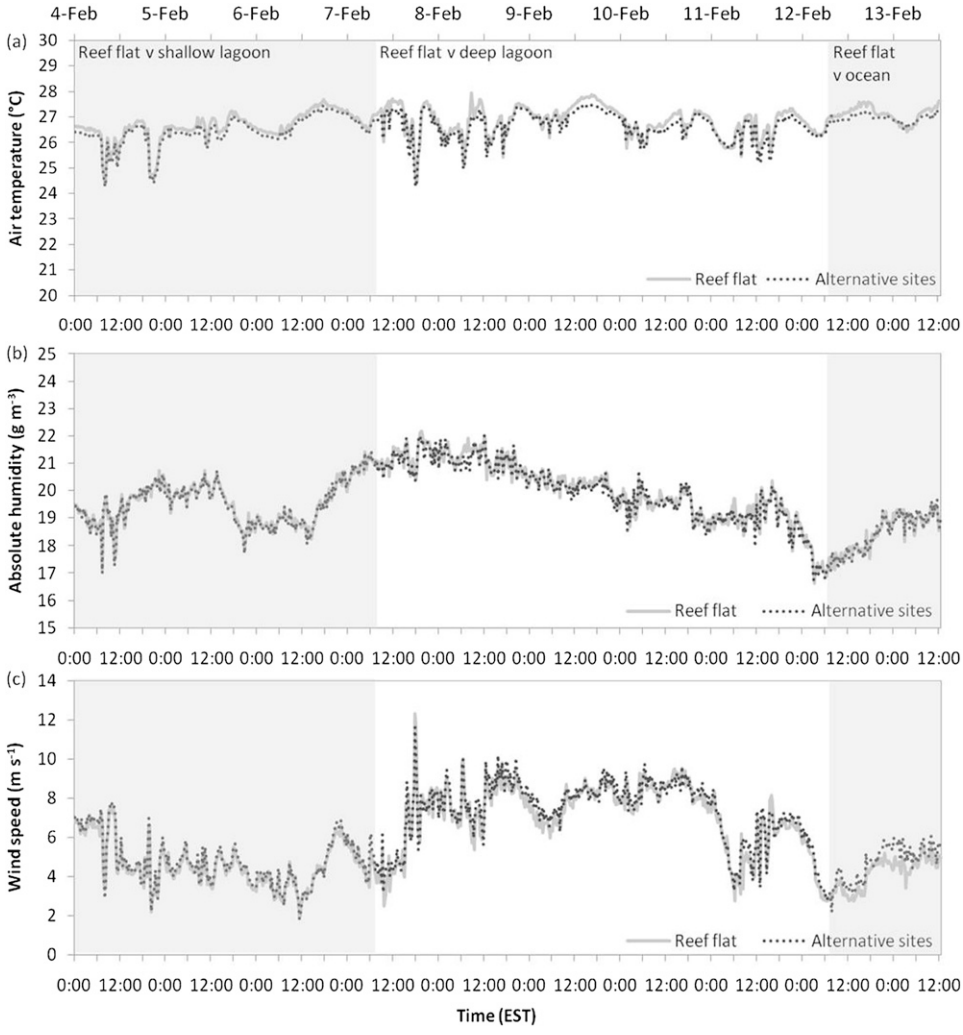

FIG. 4. (a) Air temperature, (b) absolute humidity, and (c) wind speed during the three OPs at the reef flat (smooth line), and shallow lagoon, deep lagoon, and open ocean (dashed line) from 4 to 13 Feb 2010 (OPs differentiated by shading).

b. Hydrodynamics

The tidal range at Heron Reef decreased during OP1 and then made a transition from a neap phase to a spring phase after 9 February 2010 (OP2), resulting in increasing tidal ranges (Fig. 5). During OP1, the mean water depth was 0.9 m at the reef flat and 2.7 m at the shallow lagoon (Table 3). The mean water surface temperature was 27.5°C on the reef flat during OP1, as compared with 27°C at the shallow lagoon. During OP2 the mean water surface temperature at the reef flat (27.8°C) exceeded that of the deep lagoon by 0.4°C. The smaller temperature difference between the reef flat and deep lagoon was due to heavy rainfall during OP2 (Table 3). The mean water depth at the reef flat was 1 m during OP3, as compared with 11 m at the ocean site, with average surface temperatures at the ocean and reef flat sites of 28.1° and 27.4°C, respectively. During February 2010 buoy wave data from Emu Park, to the northeast of Heron Island (provided by the Queensland Department of Environment and Resource Management), showed a mean direction of 85°, with a standard deviation of 13°, and mean significant wave height of 0.96 m. The average significant wave height was highest during OP2 (1.2 m).

c. Radiative fluxes

The relative magnitudes of short- and longwave radiation and turbulent fluxes during the study over Heron Reef are presented in Fig. 6. Spatial variation in outgoing shortwave radiation $K\uparrow$ was the key driver of zonal differences in Q^* and was dependent primarily on water depth (albedo), while outgoing longwave radiation

TABLE 3. Mean meteorological and hydrodynamic conditions over the reef flat, shallow lagoon, deep lagoon, and open ocean for the corresponding OPs.

	OP1		OP2		OP3	
	0000 UTC 4 Feb–0500 UTC 7 Feb		0530 UTC 7 Feb–0700 UTC 12 Feb		0730 UTC 12 Feb–1230 UTC 13 Feb	
Mean conditions	Reef flat	Shallow lagoon	Reef flat	Deep lagoon	Reef flat	Ocean
Water depth (m)	0.9	2.7	0.8	3.1	1	11
Water surface temperature (°C)	27.5	27.0	27.8	27.4	28.1	27.4
Evaporation (mm day^{-1})	3.0	3.6	4.9	6.8	4.05	4.13
Absolute humidity (g m^{3})	19.4	18.8	19.9	19.9	18.5	18.4
Air temperature (°C)	26.7	26.5	26.9	26.7	27.1	26.9
Wind speed (m s^{-1})	4.6	4.8	7.0	7.2	4.2	4.7
Albedo	0.11	0.10	0.15	0.10	0.11	0.04
Air–water temperature (°C)	0.8	0.5	0.8	0.6	1	0.6
Water–air vapor pressure (hPa)	6.4	6.7	6.4	6.7	9.6	9
Total rainfall (mm)	8		24.2		0	
Time cloud cover (%)	73		91		54	

$L\uparrow$ reflected water surface temperature. Net longwave radiation L^* was negative at all sites during all observation periods as $L\uparrow$ consistently exceeded $L\downarrow$. At the reef flat site, $L\uparrow$ was 10%, 12%, and 16% higher than the alternative sites during OP1, OP2, and OP3, respectively (Fig. 6). Net shortwave radiation K^* was the principal energy input at all sites for turbulent flux exchange. Each day, $K\downarrow$ peaked at around midday, coinciding with maximum solar azimuth and decreased sharply during cloudy periods such as OP2 due to the high albedo of the cloud top restricting $K\downarrow$ at the surface. Mean daytime albedos of the reef flat were 10%, 26%, and 45% higher than the shallow lagoon, deep lagoon, and ocean sites, respectively, resulting in greater $K\uparrow$ and lower overall available Q^*. Total $K\uparrow$ at the reef flat was 110%, 40%, and 5% greater than the deep ocean site during OP3, the deep lagoon during OP2, and the shallow lagoon during OP1, respectively (Table 3). Consequently, Q^* was highest (lowest) over the ocean (reef flat). At the reef flat, the water level was linearly correlated with $K\uparrow$ during all observation periods, with an average coefficient of determination

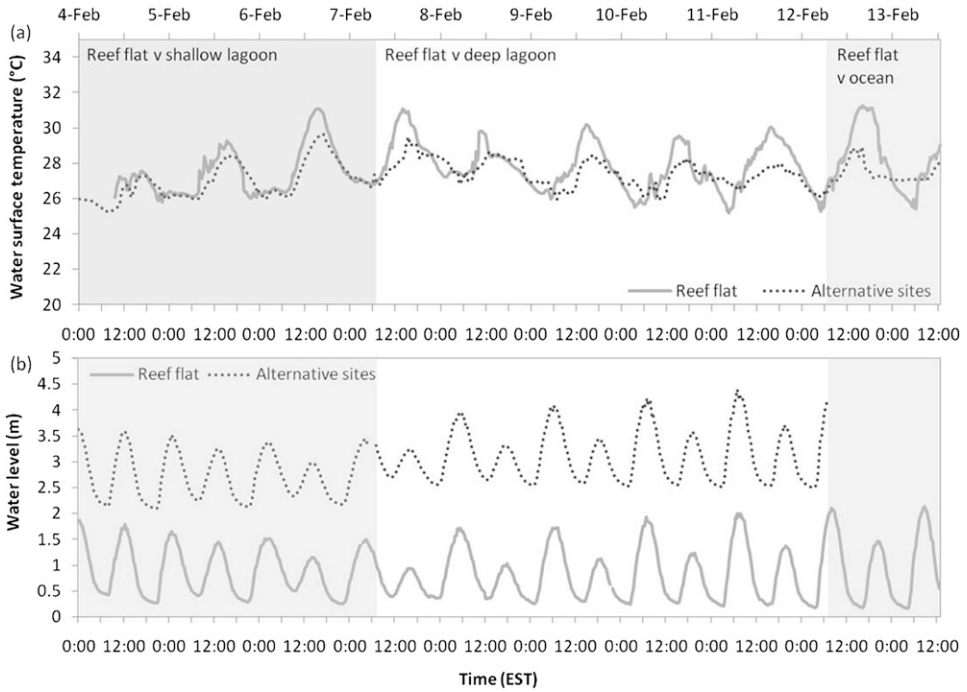

FIG. 5. As in Fig. 4, but for (a) water surface temperature and (b) water level.

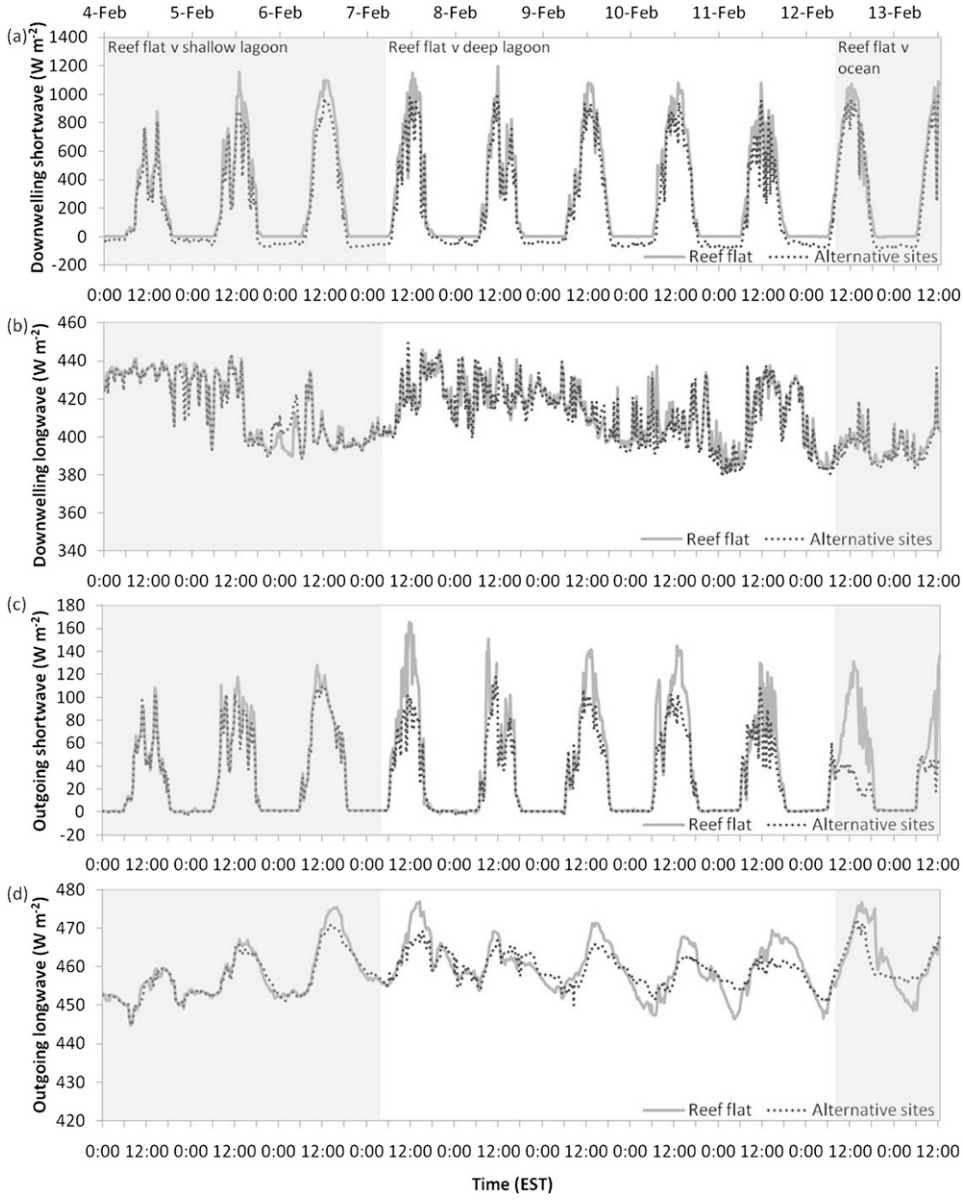

FIG. 6. The (a) $K\downarrow$, (b) $L\downarrow$, (c) $K\uparrow$, and $L\uparrow$ for the reef flat (smooth line), and shallow lagoon, deep lagoon, and open ocean (dashed line) during the three OPs from 4 to 13 Feb 2010 (delineated by numbering and shading).

(R^2) value of 0.25 due to the high reflectivity of the white coral sand on the reef flat.

During OP2, the average Q^* was 7% higher at the reef flat than OP1, increasing from an average of 165.5 to 174.6 W m^{-2}, and Q^* at the deep lagoon was 6% higher than the shallow lagoon during OP1 (Table 4). Cloud cover was present for 91% of OP2 (up from 73% during OP1) resulting in higher $L\downarrow$. Despite this, $L\uparrow$ was also higher because of warmer water surface temperatures, resulting in a slight reduction in L^* from an average of -44.9 to -49.8 W m^{-2} at the reef flat (Table 4). Net longwave radiation averaged -49.6 W m^{-2} over the deep lagoon. Higher rates of $K\downarrow$ were the primary cause of higher Q^* during OP2. The percentage of $K\downarrow$ reflected as $K\uparrow$ increased from 13% to 15% at the reef flat, due to the increasing tidal range, which resulted in a lower mean water level (0.1 m lower than OP1) and increased the albedo of white coral sand patches at low tides. This resulted in mean K^* of 226.2 W m^{-2}, while at the deep lagoon 11% of $K\downarrow$ was reflected, causing a total K^* of 238.6 W m^{-2}. Outgoing shortwave radiation was lower at the deep lagoon during OP2 than at the shallow

TABLE 4. Radiation and turbulent flux statistics for the three OPs.

	OP1		OP2		OP3	
Mean flux ($W\ m^{-2}$)	Reef flat	Shallow lagoon	Reef flat	Deep lagoon	Reef flat	Ocean site
$L\uparrow$	458.2	457.8	459.8	459.4	461.5	461
$L\downarrow$	413.3	413.6	411	409.8	395.6	394
$K\uparrow$	31.6	29.9	41.7	28.5	42.3	20
$K\downarrow$	242	248.6	267.9	267.1	369.2	390
Q^*	165.5	174.6	177.4	189.1	261	302.8
Q_E	84.9	102	138.4	191.8	115.7	117.7
Q_H	6.7	5.3	16.4	14.9	8	3.8
Q_{SWR}	73.9	67.3	22.6	−17.6	137.3	181.3
θ	0.14	0.05	0.1	0.08	0.05	0.03

lagoon during OP1 as the minimum water depth at the deep lagoon was 0.4 m higher.

After a return to more settled weather conditions during OP3, the extent of cloud cover dropped to 53%. Consequently, Q^* peaked at 904 W m^{-2} at the reef flat during OP3, as compared with an average daily maximum of 861.3 W m^{-2} during OP2, and 885.2 W m^{-2} during OP1. Lower $K\uparrow$ at the ocean site during OP3 meant that total available Q^* was 4.7 MJ m^{-2} day^{-1} higher than at the reef flat, at 33.8 MJ m^{-2} day^{-1}.

d. Turbulent fluxes

1) OVERVIEW

During the field campaign, temporal variability in Q_E, Q_H, and Q_{SWR} mainly depended on the prevailing meteorology, while site-specific hydrodynamics caused spatial divergence of fluxes. The energy storage flux peaked at around midday daily (Fig. 7), coinciding with maximum Q^*, and was moderated by the presence of cloud, indicated by sharp falls in Q_{SWR} (Fig. 7). Latent and Q_H fluxes typically reached their maximums in the evening between 1500 and 1800 EST when the air–water surface temperature gradient was highest and wind speed increased. The Q_{SWR} decreased to below zero after sunset as evaporation from the water surface continued. Consequently, daily minimums in Q_{SWR} occurred in the early evening when Q_E was highest (Fig. 7c). During OP2, Q_E and Q_H were observed to plateau under the influence of unstable, strong southeasterly conditions, before returning to similar levels to OP1 during OP3. At all study sites during the field campaign,

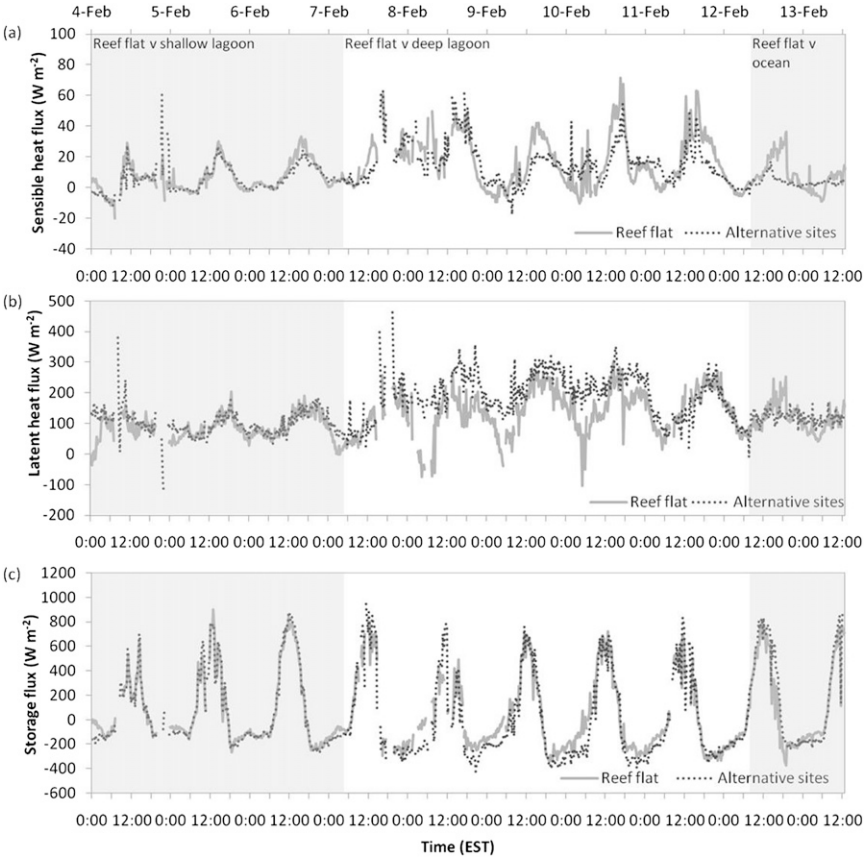

FIG. 7. As in Fig. 6, but for (a) Q_H, (b) Q_E, and (c) Q_{SWR}.

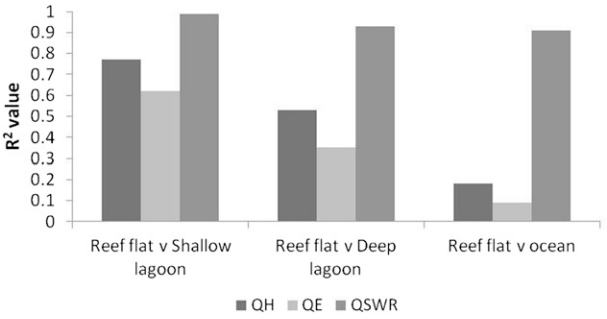

FIG. 8. The R^2 values for a linear correlation function for the turbulent fluxes Q_H, Q_E, and Q_{SWR} between the reef flat and shallow lagoon (OP1), reef flat and deep lagoon (OP2), and the reef flat and open ocean (OP3).

Q_H was low (averages < 15 W m^{-2}) with the majority of Q^* partitioned into Q_E and Q_{SWR}. Sensible heat flux was consistently higher and Q_E was generally lower at the reef flat than the other sites during all three observation periods. A lower air–seawater vapor gradient θ and lower wave action at the reef flat are likely to have resulted in less evaporation at the site. Consequently, higher β were recorded at the reef flat, where β averaged 0.14, 0.1, and 0.05 for OP1–3, respectively. Mean β values at the shallow lagoon, deep lagoon, and ocean sites were 0.05, 0.08, and 0.03, for the corresponding OPs.

2) LATENT HEAT FLUX

The dominant controls on Q_E differed at the reef flat and shallow lagoon during OP1. At the shallow lagoon, where Q_E was higher, wind was the primary driver of Q_E ($R^2 = 0.25$), whereas over the reef flat the reef–air vapor pressure difference θ was the dominant control on Q_E ($R^2 = 0.47$). Mean wave height was 0.03 m at the reef flat during OP1 and correlated weakly with evaporation ($R^2 = 0.15$). While concurrent wave data were not available for the shallow lagoon, it is likely that greater wave action due to the deeper water at the shallow lagoon site would have increased mixing (Graf et al. 1984), resulting in the higher recorded Q_E.

During OP2, the magnitude of the difference in fluxes between the reef flat and deep lagoon was more pronounced than between the reef flat and shallow lagoon during OP1. The R^2 value for a linear correlation between Q_E at the reef flat and deep lagoon was 0.35, as compared with 0.62 for the reef flat and shallow lagoon during OP1 (Fig. 8). At the start of OP2, during the morning of 7 February 2010, the wind speed was approximately 4 m s^{-1} until around 1600 EST. After this time the wind speed increased and remained at an average of 8 m s^{-1} until the evening of 10 February 2010. Prior to this wind speed increase, the mean values of Q_E were 75.9 and 79 W m^{-2} at the reef flat and deep lagoon, respectively (Fig. 7). The increase in wind speed corresponded with an increase in mean Q_E of 90% at the reef flat and 154% at the deep lagoon. Accordingly, it appears that increasing wind speed elevated Q_E at both sites, yet to a greater degree at the deep lagoon most likely due to increased wave action.

3) SENSIBLE HEAT FLUX

Sensible heat flux was highest at the reef flat during all observation periods, due to consistently warmer water surface temperatures. At the reef flat, Q_H correlated strongly with water surface temperature during OP1 and OP3 ($R^2 = 0.7$ and 0.88), and to a much lesser degree during OP2 ($R^2 = 0.24$), perhaps due to higher rainfall causing sensible heat loss from the water column. At the shallow lagoon, deep lagoon, and ocean sites, Q_H was better correlated with the air–water temperature ratio ($R^2 = 0.5$, 0.55, and 0.58), due to the thermal inertia of these deeper sites causing greater variation in this parameter. The diurnal range of Q_H was larger at the reef flat than the alternative sites because of larger fluctuations in the controlling parameters.

4) STORAGE FLUX

Energy storage was higher at the reef flat than other sites during OP1 and OP2, resulting in warmer water temperatures. It was lower at the reef flat than the ocean during OP3, however, due to a spike in Q_E at the reef flat at approximately 1500 EST on 12 February 2010, which coincided with the low tide at 1500 EST of 0.23 m. It appears that the spike resulted from high θ at the reef flat while the coral was exposed, when it reached the maximum for the three observation periods at 18 hPa, compared to 13 hPa over the ocean. In further support of this conclusion, the strongest correlation between θ and Q_E occurred at the reef flat during OP3 (R^2 of 0.62). The weakest correlation between sites for Q_E and Q_H occurred between the reef flat and ocean during OP3 (Fig. 8). This is primarily due to the previously mentioned spikes and suggests that water depth and its impact on temperature and θ can result in significant spatial differences in fluxes between the reef and ocean. Because of the brevity of OP3, extracting definitive conclusions from this dataset is difficult.

e. Total fluxes

Total heat fluxes for the four observation sites during the February 2010 field campaign are presented in Fig. 9 and illustrate that the least variation between sites occurred during OP1 because of low wind speeds, clear conditions, and similar water depths at the two measurement sites. Strengthening southeasterly winds during OP2 resulted in the greatest deviation in Q_E and

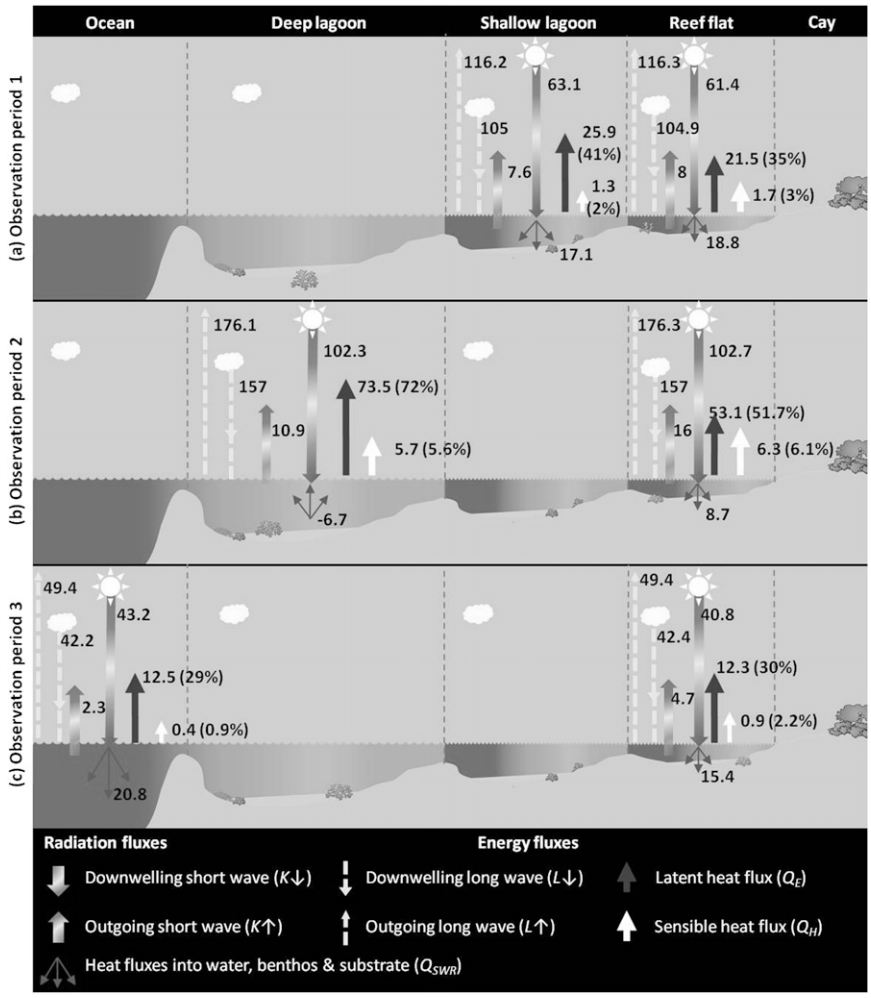

FIG. 9. Total daily fluxes (MJ m^{-2} day^{-1}) at the (a) reef flat and shallow lagoon during OP1, (b) reef flat and deep lagoon during OP2, and (c) reef flat and open ocean during OP3. Numbers in parentheses represent the fluxes as a percentage of total incident shortwave radiation.

Q_{SWR} between sites of the three observation periods. At the reef flat during OP2, the total Q_{SWR} was 8.7 MJ m^{-2} day^{-1}; yet, despite this gain of energy by the water column, from 1700 EST 7 February 2010 to 1700 EST 11 February 2010, the water surface temperature at the reef flat decreased by 0.5°C, due to rainfall. At the deep lagoon during this period, total Q_E exceeded total available Q^*, resulting in a net loss of Q_{SWR} (−6.7 MJ m^{-2} day^{-1}) as the water body became the energy source for evaporation. Consequently, the drop in water temperature due to rainfall was exacerbated by high evaporation at the deep lagoon, resulting in a greater decrease in water surface temperature than at the reef flat, of 1.3°C.

During OP2 correlation analysis indicated that θ was the key driver of Q_E at the reef flat ($R^2 = 0.39$). At the deep lagoon, however, Q_E was strongly correlated with wind speed ($R^2 = 0.69$) and the relationship with θ was negligible ($R^2 = 0.07$). Furthermore, during OP3 when the difference in θ between the reef flat and open-ocean sites was the largest of the three observation periods (0.6 hPa as compared with 0.3 hPa during OP1 and OP2), total Q_E was only 0.2 MJ m^{-2} day^{-1} larger at the ocean site. This meant that the total Q_E as a proportion of $K\downarrow$ at the ocean was only 1% higher than at the reef flat. During OP2, Q_E accounted for 21% more of $K\downarrow$ at the deep lagoon (at 72%) than the reef flat (51%), indicating that θ influenced Q_E less than wind and its related effects (wind waves and, potentially, sea spray) (Makin 1998).

Wind waves and sea spray increase the flux of water between the sea surface and the atmosphere by increasing the eddy diffusivity and mixing (McJannet et al. 2012). Brander et al. (2004) showed that wave

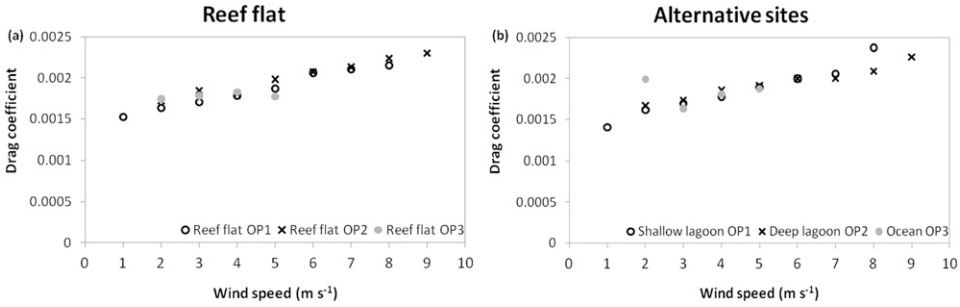

FIG. 10. Mean neutral drag coefficient vs wind speed for the (a) reef flat and (b) alternative sites during OP1 (open circles), OP2 (crosses), and OP3 (shaded circles).

height and type were both strongly wind and depth dependent; that maximum wave heights occurred during high tide; and that wind waves did not develop at water levels of <1 m. Thus, while no wave data were available for the deep lagoon during OP2, it is reasonable to deduce that during OP2 the difference in water depth between the reef flat (average 0.8 m) and deep lagoon (average 3.1 m) resulted in greater wave action at the latter site, exacerbating the wind-driven increase in evaporation at that site.

f. Momentum flux

The drag coefficient C_D, which represents the total air–sea momentum flux (Hasse and Smith 1997), was calculated for the measurement height of 2.2 m and corrected for stability following Hsu (1988). The resulting C_D ranged from 1.5×10^{-3} to 2.3×10^{-3} for all sites (Fig. 10). No site-specific tendency was observed as C_D is primarily a function of wind speed, which was similar at all sites (Hasse and Smith 1997). The drag coefficients were the same at both the reef flat and shallow lagoon during OP1, at 1.85×10^{-3}. They were 2×10^{-3} and 1.9×10^{-3} at the reef flat and deep lagoons, respectively, during OP2 and 1.78×10^{-3} and 1.82×10^{-3} during OP3 at the reef flat and deep lagoon. At a height of 10 m the drag coefficient C_{DN} was lower at 1.3×10^{-3} (reef flat and shallow lagoon) during OP1, 1.52×10^{-3} (reef flat) and 1.47×10^{-3} (deep lagoon) during OP2, and 1.34×10^{-3} (reef flat and ocean) during OP3. Throughout the observation periods the stability parameter z/L was consistently < 0, indicating unstable conditions throughout the daytime. The drag coefficient was found to correlate positively with z/L, albeit weakly, with the surface drag generally increasing during unstable conditions ($z/L < 0$) as enhanced turbulence increased sea surface roughness (Sun et al. 2001).

6. Discussion

This study presented results from the first concurrent in situ EC measurements of surface radiation, heat, and moisture exchanges over different geomorphic zones at Heron Reef, and the adjacent deeper ocean. In doing so it contributes to the understanding of air–reef–water surface energy fluxes over coral reefs, which have previously been described by single-point measurements only, often made from shoreline locations. While providing insight into energy exchanges across the reef–atmosphere interface, such studies have typically been restricted to specific meteorological conditions such as onshore winds only, or have been confined to a specific location on a reef and therefore have not described the spatial variability in energy exchanges over the different geomorphic and benthic zones found on coral reefs.

The energy fluxes presented here for the reef flat site (mean depth 0.9 m) were within the range of those previously reported for coral reef flats, although direct comparison is difficult due to inconsistencies in the presentation of flux data between studies. The mean Q^* ranged from 165 to 261 W m^{-2}, which was generally in agreement with summertime Q^* reported for coral reefs (Kjerfve 1978; Tanaka et al. 2008). The mean Q_H and Q_E over the reef flat for the three observation periods ranged from 6.7 to 16.4 W m^{-2} and from 84.9 to 138.4 W m^{-2}, respectively. These results were similar to values reported by Tanaka et al. (2008), who measured the mean Q_H and Q_E to be 6 and 60 W m^{-2} at Japan's Miyako Island. McCabe et al. (2010) calculated mean Q_E using bulk formulas over the reef flat at Lady Elliot Island, south of Heron Reef, to be 150–250 W m^{-2} during autumn, when cooler winds facilitate higher extraction of heat from the water surface and higher evaporation would be expected. Results from the reef flat site in the present study were compared with others in Table 5. The mean β over the reef flat ranged from 0.05 to 0.14 and was higher than the lagoon and ocean sites because of higher Q_H over the warmer, shallower water of the reef flat. Similar values were reported for winter and spring conditions over the reef flat at Heron Island by McGowan et al. (2010). In comparison, Garratt and Hyson (1975) reported β values of 0.19–0.2 over coral plateaus in the

TABLE 5. Summary of Q^*, Q_H, and Q_E fluxes (W m^{-2}), and the neutral drag coefficient corrected for a height of 10 m, in previous studies and in the present study at the reef flat site. Latent heat flux data from McCabe et al. (2010) were as reported before a distinct atmospheric transition and Q_H was estimated from Fig. 8. Tanaka et al. (2008) data were from their Table 4. Kjerfve's (1978) Q_E were as reported and the Q_H was estimated from Fig. 3. The Q_H for Hicks (1972) was estimated from Fig. 5, and for Smith (2001) Q^* and Q_H were estimated from Fig. 3 and Q_E was reported. For Garratt and Hyson (1975), Q_H and Q_E were reported. Here, BF is bulk formula and N/A indicates not available.

Reference	Method	Depth (m)	Season	Q^*	Q_H	Q_E	$C_{DN} \times 10^{-3}$
Present study	EC	1	Summer	201	10	113	1.4
McCabe et al. (2010)	BF	< 2	Autumn	N/A	<25	150	N/A
Tanaka et al. (2008)	EC	<10	Summer	223	6	60	N/A
Kjerfve (1978)	BF	<1	Summer	124	56	202	N/A
Hicks (1972)	EC	<3	Spring	N/A	~25	N/A	0.79
Smith (2001)	BF	4	Summer	~170	~0	29	N/A
Garratt and Hyson (1975)	EC	4–7	Winter	N/A	110	550	1.5

East China Sea, which they attributed to cold-air advection, driving Q_H.

The relative partitioning of energy budget parameters across all sites at Heron Reef was similar, yet the individual magnitudes were different at each site. During daylight hours solar radiation was the key energy input that drove heat and moisture fluxes across the reef–air interface. Net radiation was found to vary in response to water depth, with higher $K\uparrow$ over shallower water due to less attenuation of light by the water column and higher albedo of the white coral sand at this site. Both Q^* and Q_{SWR} peaked at around midday on clear sunny days and were moderated by the passage of cloud cover, as described by Smith (2001). The storage heat flux was also moderated by wind speed, which increased evaporation from the reef water surface. Cloud cover was a key control of $K\downarrow$ and, in addition to wind speed, the water temperature of the different geomorphic zones. Low levels of both wind speed and cloud cover and high solar radiation have been shown to be principal factors during localized coral bleaching (MacKellar and McGowan 2010). Diminished DMS production by coral reefs under thermal stress may also exacerbate the threat of bleaching under certain meteorological conditions by inhibiting cloud development by reducing cloud condensation nuclei and, thus, enhancing solar radiation (Jones et al. 2007).

A positive correlation between wind and evaporation was measured at all sites, with stronger correlations recorded at the deeper sites. This was evident during OP2, when an increase in Q_E corresponding with an increase in mean wind speed of 3 m s^{-1} was exacerbated at the deep lagoon. This caused a net loss of heat from the water surface as Q_E exceeded Q^*, while a net relative gain of Q_{SWR} occurred at the reef flat. Consequently, under similar meteorological conditions the reef flat was a net sink of energy, while the deep lagoon was a source of heat to the atmosphere. The θ was stronger during OP3 than OP2, indicating that wind-driven forces influenced evaporation during OP2. As wave height and type are directly correlated with wind speed and water depth, it appeared that enhanced wave action (wave height, wind waves and sea spray) at the deep lagoon exacerbated Q_E at the deep lagoon.

In contrast to Q_E, Q_H was consistently higher at the reef flat than the deeper sites, due to higher water temperatures (on average 0.55°C higher). These results highlighted the ability of moist, unstable southeasterly air masses at Heron Reef, which are common to the region during summertime, to suppress solar heating (via increased cloud cover) and increase evaporation (via higher wind speeds). It was also a key example of how the surface energy balance varies within a relatively short distance across a coral reef.

During OP3, no significant difference in total evaporation was observed between the reef flat and the ocean site. The surface roughness length was higher at the reef flat than the ocean site, likely due to exposure of coral heads during low tides. Minimum water level at the reef flat was 0.2 m at 1600 EST on 12 February. This resulted in very high water temperatures and θ that, in conjunction with the exposure of coral, were thought to be responsible for an unexpected spike in Q_E. The brevity of OP3, however, limited conclusive elucidation of these findings, and future research will aim to undertake a longer comparison between the ocean and reef energy balances.

Important is that this study shows that hydrodynamic differences between the geomorphic zones at Heron Reef resulted in variations in energy exchanges across the water surface–air interface. This paper confirms that single measurement sites cannot be considered representative of entire reefs and may therefore be insufficient for determining the role of coral reefs in atmospheric processes. Marked variations in surface characteristics, hydrodynamics, and consequently the energy balance parameters, occurred at spatial and temporal scales smaller

than those previously measured using remotely sensed air–sea energy fluxes along the GBR. Weller et al. (2008), for example, used remotely sensed input parameters and bulk algorithms to derive a heat budget of the GBR and Coral Sea. Their results were monthly estimates of the surface heat budget at a spatial resolution of 4 km^2. Our findings have highlighted, however, distinct differences in the surface heat budget at the geomorphic scale (hundreds of meters) and over periods ranging from hours to days. In situ measurements of fluxes may, therefore, assist in the calibration of remotely sensed measurements. Furthermore, research that has used single-point measurements of energy exchanges over coral reefs (McCabe et al. 2010; Tanaka et al. 2008) are only accurate at the geomorphic zone scale, rather than the reef scale at which their findings are often purported to represent. Accordingly, our results have provided insight into the variability of radiation and turbulent fluxes that are likely to exist over reefs with different geomorphic assemblages, such as shallow reef plateaus compared to lagoon-dominated reefs.

The mean drag coefficients ranged from 1×10^{-3} to 2.5×10^{-3}, with only minor differences between sites. The drag coefficient increased as a function of wind speed, a dependency that has been observed at moderate wind speeds over the open ocean (Foreman and Emeis 2010; Smith and Banke 1975; Wu 1969), shallow coastal environments (Tsukamoto et al. 1991), and coral reefs (Garratt and Hyson 1975). At wind speeds < 5 m s^{-1}, the C_D over the ocean during OP3 was comparable to the reef flat site, although measurements are required under a wider range of wind speeds and tides to accurately establish differences between the open ocean and coral reef. Hicks (1972) observed no difference between shallow and deep water, while Tsukamoto et al. (1991), who measured C_D as 1.69×10^{-3} over a coastal zone (4 m) off a pier in the Sea of Japan, potentially identified an increase in C_D over deeper (10 m) water but could not separate the depth and wind dependencies.

The computed drag coefficient C_{DN} for a height of 10 m under neutral conditions yielded values of between 1.1 and 1.7×10^{-3}, with an average of 1.4×10^{-3}. These values are in good agreement with those reported over oceans and lakes, which typically range from 1×10^{-3} to 2×10^{-3} (Dunckel et al. 1974). Direct comparison with previous C_{DN} results over coral reefs was difficult as those available for comparison were measured during winter cold-air outbreaks (Garratt and Hyson 1975) or when biological factors were thought to be an influence (Hicks 1972). Garratt and Hyson (1975) found a C_{DN} of 0.5×10^{-3}–2×10^{-3} and attributed large scatter in their coefficients to the influence of the coral plateau, breaking waves on the reef rim, or flow distortion due to local topography and islands upwind. Hicks (1972) found that C_{DN} was identical over a shallow lake (7 m) and adjacent ocean, indicating that momentum flux was not influenced by long-wave properties present in large water bodies as the ocean. Hicks et al. (1974) later measured C_{DN}, the Reynolds stress, and Q_H downwind from a shallow coral reef (depth < 3 m) off the coast of Papua New Guinea during spring. At Hicks's site C_{DN} was close to an aerodynamically smooth surface and the derived Stanton number (1.1×10^{-3}) was lower than would be expected over deeper water (1.5×10^{-3}). Consequently, the bulk coefficients derived over the open ocean overestimated Q_H at the reef site. The smoothness of the surface was attributed to the presence of a surface film of coral secretions (Deacon 1979).

There is a lack of data on the aerodynamic roughness of coral reefs and, even recently, work on gas exchange over coral reefs has relied on C_{DN} for lakes. Abe et al. (2010) employed the C_{DN} (1.2×10^{-3}) from an 8-m-deep site at Lake Hefner, Oklahoma (Emmanuel 1975), to estimate gas transfer over Kabira Reef, Japan (depth < 2.5 m). Yet, at Lake Toba in Indonesia, Sene et al. (1991) found a C_{DN} of 1.8×10^{-3}. Thus, while C_{DN} values over lakes, oceans, and coral plateaus appear to fall within the range of 1×10^{-3}–2×10^{-3}, bulk coefficients appear to be time and site specific (Frederickson et al. 1997). Clearly, further studies are required to obtain a comprehensive dataset of the turbulent transfer of momentum, heat, and water vapor over coral reefs under a full suite of meteorological and hydrodynamic conditions.

To understand the role of coral reefs in regional weather and climate and the likely impacts of climate change on the state of the reef systems, it is important that radiation and turbulent fluxes are parameterized at a sufficient resolution to ensure that coral reefs are accurately represented in GCMs. Not only is there a dearth of research on air–reef–water surface energy exchanges, but the present study has highlighted significant variations in interfacial fluxes between the key geomorphic zones at Heron Reef. Consequently, there is a need for further in situ EC measurements of air–reef–water surface fluxes to clarify the role of coral reefs in energy budgets larger than the reef scale, and calibrate remotely sensed and modeled energy flux transfers over coral reefs. This is particularly pertinent in an era when the future of coral reefs under a global warming climate change scenario is a topic of great contention (Hoegh-Guldberg 1999). Furthermore, understanding the spatial variation in radiation and energy fluxes across coral reef geomorphic zones may lead to a better

understanding of spatial and temporal ''patchiness'' of coral bleaching within coral reefs (McCabe et al. 2010). With coral bleaching episodes trending upward in number and scale with global temperatures, particularly in the past 30 yr (Glynn 1993), an understanding of the key controls on coral bleaching is crucial. While Q_{SWR} was determined as the residual of the energy budget equation and, thus, care must be taken when interpreting results, the relative magnitudes of the energy budget parameters in our results are consistent with the findings of previous research (Nihei et al. 2002; Tanaka et al. 2008).

7. Conclusions and future research

Accurate measurements of radiation transfers and the fluxes of heat, moisture, and momentum over various geomorphic zones of a coral reef are important for understanding the driving forces behind local to regional weather and hydrodynamics, elucidating the controls of coral bleaching; improving prediction of climate change–related impacts on coral reefs, as well as parameterization of the role of coral reefs in climate models. The resolution and/or aspatial nature of previous research on air–reef–water surface fluxes has been insufficient to accurately capture spatial heterogeneities across the reef zones, rather using single-point measurements, which are at too fine of a resolution (single zone), or remotely sensed data, which are too coarse. Accordingly, this paper presents a unique dataset of concurrent in situ EC measurements made at Heron Reef, in the southern Great Barrier Reef.

Results highlight key differences in the relative magnitudes of the individual fluxes between sites, under various meteorological conditions. Available net radiation peaked around midday on clear days and was moderated by cloud cover, which increases cloud-top albedo. Net radiation was lowest over the shallow reef flat, where less attenuation of light by the water column results in higher albedo of the white coral sand. Accounting for a significant portion of available net radiation, storage flux was also moderated by cloud cover, in addition to wind speed (via evaporative cooling of the water). This meant that more energy was available for the interfacial fluxes at the deeper sites. Sensible heat flux was consistently higher over the reef flat, where the shallow water was warmer and the water surface–air temperature ratio was the highest. Conversely, evaporation was higher at the deeper water sites, where the water surface–air vapor pressure difference and wind–wave effects were greater.

The magnitude of the difference in fluxes between sites increased with wind speed, as was observed during the second observation period when an increase in wind speed, associated with unstable southeasterly trade winds, enhanced evaporation over the deep lagoon. Consequently, during this period the deep lagoon was a source of energy to the atmosphere, while the reef flat remained a sink. This research has made an important finding that the interfacial fluxes behaved very differently over the different geomorphic zones, and that the characteristics of variation depend on meteorology and hydrodynamics. Measurements over longer time periods and under a wider range of meteorological conditions and seasons are required to fully quantify zonal variation in air–reef–water surface fluxes, and over the adjacent open ocean. The next phase of this research will involve more accurate parameterization of the heat fluxes within the water column, in order to accurately account for the effects of advection due to currents and flushing across Heron Reef. It will also include measurements of air–reef–water surface fluxes over different reefs characterized by different geomorphic zones elsewhere.

Acknowledgments. The authors acknowledge the financial and technical support provided by the School of Geography, Planning and Environmental Management, University of Queensland. We thank J. Soderholm, G. Ewels, and the staff of the Heron Island Research Station for assistance during the field campaign. We also acknowledge the GBRMPA for allowing our research at Heron Reef, Permit G09/3033.1.

REFERENCES

Abdella, K., and S. D'Alessio, 2003: A parameterization of the roughness length for the air–sea interface in free convection. *Environ. Fluid Mech.,* **3,** 55–77.

Abe, O., A. Watanabe, V. V. S. S. Sarma, Y. Matsui, H. Yamano, N. Yoshida, and T. Saino, 2010: Air–sea gas transfer in a shallow, flowing and coastal environment estimated by dissolved inorganic carbon and dissolved oxygen analyses. *J. Oceanogr.,* **66,** 363–372.

Ahmad, W., and D. Neil, 1994: An evaluation of Landsat Thematic Mapper (TM) digital data for discriminating coral reef zonation: Heron Reef (GBR). *Int. J. Remote Sens.,* **15,** 2583–2597.

Allen, G. A., L. S. Pereira, T. A. Howell, and M. E. Jensen, 2011: Evapotranspiration information reporting: I. Factors governing measurement accuracy. *Agric. Water Manage.,* **98,** 899–920.

Andrefouet, S., and C. Payri, 2001: Scaling-up carbon and carbonate metabolism of coral reefs using in-situ data and remote sensing. *Coral Reefs,* **19,** 259–269.

Arya, S. P., 2001: *Introduction to Micrometeorology.* Academic Press, 420 pp.

Beyrich, F., and Coauthors, 2002: Experimental determination of turbulent fluxes over the heterogeneous LITFASS area: Selected results from the LITFASS-98 experiment. *Theor. Appl. Climatol.,* **73,** 19–34.

Brander, R. W., P. S. Kench, and D. Hart, 2004: Spatial and temporal variations in wave characteristics across a reef platform, Warraber Island, Torres Strait, Australia. *Mar. Geol.,* **207,** 169–184.

Bureau of Meteorology, cited 2011: *Climate.* Bureau of Meteorology, Commonwealth of Australia. [Available online at http://www.bom.gov.au.]

Charlson, R. J., J. E. Lovelock, M. O. Andreae, and S. G. Warren, 1987: Oceanic phytoplankton, atmospheric sulphur, cloud albedo and climate. *Nature,* **326,** 655–661.

Chen, D., and A. Krol, 1997: Hydrogeology of Heron Island, Great Barrier Reef, Australia. *Geology and Hydrogeology of Carbonate Islands. Developments in Sedimentology,* H. L. Vacher and T. Quinn, Eds., Elsevier Science, 867–884.

Deacon, E. L., 1979: The role of coral mucus in reducing the wind drag over coral reefs. *Bound.-Layer Meteor.,* **17,** 517–521.

DERM, 2004: Wave data recording program: Queensland wave climate annual summary for season 2003-04. Coastal Services Data Rep. 2005.1, Dept. of Environment and Resource Management, Environmental Protection Agency, Queensland Government, Brisbane, QLD, Australia, 123 pp.

Dunckel, M., L. Hasse, L. Krügermeyer, D. Schriever, and J. Wucknitz, 1974: Turbulent fluxes of momentum, heat and water vapor in the atmospheric surface layer at sea during ATEX. *Bound.-Layer Meteor.,* **6,** 81–106.

Emmanuel, C., 1975: Drag and bulk aerodynamic coefficients over shallow water. *Bound.-Layer Meteor.,* **8,** 465–474.

Fairall, C. W., E. F. Bradley, D. P. Rogers, J. B. Edson, and C. S. Young, 1996: Bulk parameterization of the air–sea fluxes for Tropical Ocean-Global Atmosphere Coupled Ocean-Atmosphere Response Experiment. *J. Geophys. Res.,* **101** (C2), 3747–3764.

Foreman, R., and S. Emeis, 2010: Revisiting the definition of the drag coefficient in the marine atmospheric boundary layer. *J. Phys. Oceanogr.,* **40,** 2325–2332.

Francey, R., and J. Garratt, 1979: Is an observed wind-speed dependence of AMTEX '75 heat-transfer coefficients real? *Bound.-Layer Meteor.,* **16,** 249–260.

Frederickson, P., K. Davidson, and J. Edson, 1997: A study of wind stress determination methods from a ship and an offshore tower. *J. Atmos. Oceanic Technol.,* **14,** 822–834.

Garratt, J., and P. Hyson, 1975: Vertical fluxes of momentum, sensible heat and water vapour during the air mass transformation experiment (AMTEX) 1974. *J. Meteor. Soc. Japan,* **53,** 149–160.

Glynn, P. W., 1993: Coral-reef bleaching—Ecological perspectives. *Coral Reefs,* **12,** 1–17.

Gourlay, M. R., 1996: Wave set-up on coral reefs. 1. Set-up and wave-generated flow on an idealised two dimensional horizontal reef. *Coastal Eng.,* **27,** 161–193.

——, and J. L. F. Hacker, 1999: Influence of waves and winds on reef-top currents at Heron Island, southern Great Barrier Reef. *Proc. 14th Australasian Coastal and Ocean Engineering Conf. and 7th Australasian Port and Harbour Conf.,* Perth, WA, Australia, Engineers Australia, 222–227.

Graf, W., N. Merzi, and C. Perrinjaquet, 1984: Aerodynamic drag: Measured at a nearshore platform on Lake of Geneva. *Meteor. Atmos. Phys.,* **33,** 151–173.

Hasse, L., and S. D. Smith, 1997: Local sea surface wind, wind stress, and sensible and latent heat fluxes. *J. Climate,* **10,** 2711–2724.

Hicks, B. B., 1972: Some evaluations of drag and bulk transfer coefficients over water bodies of different sizes. *Bound.-Layer Meteor.,* **3,** 201–213.

——, R. L. Drinkrow, and G. Grauze, 1974: Drag and bulk transfer coefficients associated with a shallow water surface. *Bound.-Layer Meteor.,* **6,** 287–297.

Hoegh-Guldberg, O., 1999: Climate change, coral bleaching and the future of the world's coral reefs. *Mar. Freshwater Res.,* **50,** 839–866.

——, and Coauthors, 2007: Coral reefs under rapid climate change and ocean acidification. *Science,* **318,** 1737–1742.

Hopley, D., S. G. Smither, and K. E. Parnell, 2007: *Geomorphology of the Great Barrier Reef.* Cambridge University Press, 532 pp.

Horst, T. W., and J. C. Weil, 1992: Footprint estimation for scalar flux measurements in the atmospheric surface layer. *Bound.-Layer Meteor.,* **59,** 279–296.

Hsu, S. A., 1988: *Coastal Meteorology.* Academic Press, 260 pp.

Isaac, P. R., 2004: Estimating surface–atmosphere exchange at regional scales. Ph.D. thesis, Flinders University of Southern Australia, 18 pp.

Jell, J. S., and P. G. Flood, 1978: Guide to the geology of reefs of the Capricorn and Bunker Groups, Great Barrier Reef Province (with special reference to Heron Reef). Dept. of Geology Papers, Vol. 8, University of Queensland, 85 pp.

Jones, G., M. Curran, A. Broadbent, S. King, E. Fischer, and R. Jones, 2007: Factors affecting the cycling of dimethylsulfide and dimethylsulfoniopropionate in coral reef waters of the Great Barrier Reef. *Environ. Chem.,* **4,** 310–322.

Kjerfve, B., 1978: Diurnal energy balance of a Caribbean barrier reef environment. *Bull. Mar. Sci.,* **28,** 137–145.

Krishna, K. M., and S. R. Rao, 2009: Study of the intensity of super cyclonic storm GONU using satellite observations. *Int. J. Appl. Earth Obs. Geoinf.,* **11,** 108–113.

Kurasawa, Y., K. Hanawa, and Y. Toba, 1983: Heat balance of the surface layer of the sea at Ocean Weather Station T. *J. Oceanogr.,* **39,** 192–202.

Large, W., and S. Pond, 1981: Open ocean momentum flux measurements in moderate to strong winds. *J. Phys. Oceanogr.,* **11,** 324–336.

Launiainen, J., 1995: Derivation of the relationship between the Obukhov stability parameter and the bulk Richardson number for flux profile studies. *Bound.-Layer Meteor.,* **76,** 165–179, doi:10.1007/BF00710895.

Lee, X., J. Finnigan, and K. Paw U, 2004: Coordinate systems and flux bias error. *Handbook of Micrometeorology: A Guide for Surface Flux Measurement and Analysis,* X. Lee, W. Massman, and B. Law, Eds., Atmospheric and Oceanographic Sciences Library, Vol. 29, Kluwer Academic, 33–66.

MacKellar, M., and H. McGowan, 2010: Air–sea energy exchanges measured by EC during a localised coral bleaching event, Heron Reef, Great Barrier Reef, Australia. *Geophys. Res. Lett.,* **37,** L24703, doi:10.1029/2010GL045291.

Makin, V., 1998: Air–sea exchange of heat in the presence of wind waves and spray. *J. Geophys. Res.,* **103,** 1137–1152.

Masiri, I., M. Nunez, and E. Weller, 2008: A 10-year climatology of solar radiation for the Great Barrier Reef: Implications for recent mass coral bleaching events. *Int. J. Remote Sens.,* **29,** 4443–4462.

Massman, W. J., and X. Lee, 2002: Eddy covariance flux corrections and uncertainties in long-term studies of carbon and energy exchanges. *Agric. For. Meteor.,* **113,** 121–144.

McCabe, R., P. Estrade, J. Middleton, W. Melville, M. Roughan, and L. Lenain, 2010: Temperature variability in a shallow, tidally-isolated coral reef lagoon. *J. Geophys. Res.,* **115,** C12011, doi:10.1029/2009JC006023.

McGowan, H. A., A. P. Sturman, M. C. MacKellar, A. H. Wiebe, and D. T. Neil, 2010: Measurements of the local energy balance over a coral reef flat, Heron Island, southern Great

Barrier Reef, Australia. *J. Geophys. Res.,* **115,** D19124, doi:10.1029/2010JD014218.

McJannet, D. L., I. T. Webster, and F. J. Cook, 2012: An area-dependent wind function for estimating open water evaporation using land-based meteorological data. *Environ. Model. Software,* **31,** 76–83, doi:10.1016/j.envsoft.2011.11.017.

Nihei, Y., K. Nadaoka, Y. Tsunashima, Y. Aoki, and K. Wakaki, 2002: Field-observation analysis of sea-bottom effects on thermal environments in a coral reef. *12th Int. Offshore and Polar Engineering Conf.,* Kyushu, Japan, Int. Society of Offshore and Polar Engineers, 362–367.

Oke, T. R., 1978: *Boundary Layer Climates.* 2nd ed. Routledge, 435 pp.

Phinn, S. R., C. Roelfsema, and P. Mumby, 2011: Multi-scale, object-based image analysis for mapping geomorphic and ecological zones on coral reefs. *Int. J. Remote Sens.,* **33,** 3768–3797.

Schmid, H. P., 1994: Source areas for scalars and scalar fluxes. *Bound.-Layer Meteor.,* **67,** 293–318.

Sene, K., J. Gash, and D. McNeil, 1991: Evaporation from a tropical lake: Comparison of theory with direct measurements. *J. Hydrol.,* **127,** 193–217.

Smith, N., 2001: Weather and hydrographic conditions associated with coral bleaching: Lee Stocking Island, Bahamas. *Coral Reefs,* **20,** 415–422.

Smith, S. D., and E. Banke, 1975: Variation of the sea surface drag coefficient with wind speed. *Quart. J. Roy. Meteor. Soc.,* **101,** 665–673.

——, and Coauthors, 1992: Sea surface wind stress and drag coefficients: The HEXOS results. *Bound.-Layer Meteor.,* **60,** 109–142.

Stammer, D., K. Ueyoshi, A. Köhl, W. Large, S. Josey, and C. Wunsch, 2004: Estimating air–sea fluxes of heat, freshwater, and momentum through global ocean data assimilation. *J. Geophys. Res.,* **109,** C05023, doi:10.1029/2003JC002082.

Stull, R. B., 2000: *Meteorology for Scientists and Engineers.* Brooks/Cole, 502 pp.

Sturman, A., and H. McGowan, 1999: Climate. *The Pacific Islands: Environment and Society,* M. Rapaport, Ed., Bess Press, 3–18.

Sun, J., D. Vandemark, L. Mahrt, D. Vickers, T. Crawford, and C. Vogel, 2001: Momentum transfer over the coastal zone. *J. Geophys. Res.,* **106** (D12), 12 437–12 448.

Tanaka, H., T. Hiyama, and K. Nakamura, 2008: Turbulent flux observations at the tip of a narrow cape on Miyako Island in Japan's southwestern islands. *J. Meteor. Soc. Japan,* **86,** 649–667.

Tsukamoto, O., and H. Ishida, 1995: Turbulent flux measurements and energy budget analysis over the equatorial Pacific during TOGA-COARE IOP. *J. Meteor. Soc. Japan,* **73,** 557–568.

——, E. Ohtaki, Y. Iwatani, and Y. Mitsuta, 1991: Stability dependence of the drag and bulk transfer coefficients over a coastal sea surface. *Bound.-Layer Meteor.,* **57,** 359–375.

——, H. Ishida, and Y. Mitsuta, 1995: Surface energy balance measurements around Ocean Weather Station-T during OMLET/WCRP. *J. Meteor. Soc. Japan,* **73,** 13–23.

Webb, E. K., G. I. Pearman, and R. Leuning, 1980: Correction of flux measurements for density effects due to heat and water vapour transfer. *Quart. J. Roy. Meteor. Soc.,* **106,** 85–100.

Weibe, A., A. Sturman, and H. McGowan, 2011: Wavelet analysis of atmospheric turbulence over a coral reef flat. *J. Atmos. Oceanic Technol.,* **28,** 698–708.

Weller, E., M. Nunez, G. Meyers, and I. Masiri, 2008: A climatology of ocean–atmosphere heat flux estimates over the Great Barrier Reef and Coral Sea: Implications for recent mass coral bleaching events. *J. Climate,* **21,** 3853–3871.

Wettle, M., A. G. Dekker, and V. E. Brando, 2005: Monitoring bleaching of tropical coral reefs from space: A feasibility study using a physics based remote sensing approach. CSIRO Wealth from Oceans Flagship Program Rep., Canberra, ACT, Australia.

Wu, J., 1969: Wind stress and surface roughness at air–sea interface. *J. Geophys. Res.,* **74,** 444–455.